IEEE Access
Multidisciplinary | Rapid Review | Open Access Journal

Received 19 July 2023, accepted 31 July 2023, date of publication 3 August 2023, date of current version 9 August 2023.

Digital Object Identifier 10.1109/ACCESS.2023.3301565

RESEARCH ARTICLE

High Reliable Lead Wire System of the Rotor Winding in Pumped Storage Power Stations

YUNHAN ZHANG[1], TAO LIU[2], KAIPING YUAN[2], AND TIELIANG LV[1]
[1]School of Microelectronics, Fudan University, Shanghai 200433, China
[2]Frontier Institute of Chip and System, Fudan University, Shanghai 200433, China

Corresponding author: Tieliang Lv (tl_l@fudan.edu.cn)

This work was supported in part by the National Key Research and Development Program of China under Grant 2021YFB3201903 and in part by the National Natural Science Foundation of China under Grant 62104045.

ABSTRACT Hydro-generators in pumped storage power stations (PSPSs) consist of multiple rotor windings connected by lead wires, which are consistently subjected to large stress due to the frequent starting and stopping, making fatigue fractures of these lead wires common. This paper proposes a fault early warning system featuring a dual-connection lead wire and a real-time fracture monitoring system to ensure high reliability of the lead wire. A fatigue testing machine is developed and the reliability of real-time fracture monitoring mechanism is proved through the validity test on this machine. Subsequently, through analysis based on the *P-S-N* model, the relationship between the fatigue life of the lead wire and the displacement amplitude of the external force it withstands was studied. This relationship can be used to predict the redundant time of dual-connection lead wires, providing reference for maintenance personnel to schedule shutdowns for generators. Conversely, this relationship can also guide lead wire designers to quantitatively adjust the expected redundant time by adjusting the lead wire's structure, to meet the needs of practical applications.

INDEX TERMS Fatigue life prediction, lead wire, pumped storage power station, rotor, high reliability.

I. INTRODUCTION

Concerns about peak oil and climate change have led many countries to mandate targets for renewable generation [1]. In China, annual hydropower generation capacity theoretically reaches 0.6 billion kWh. In the 21st Century, the world has seen high-speed development of hydropower construction in China [2]. Meanwhile, the electrified society relies increasingly on stable and reliable electricity grid. Pumped storage power station (PSPS) is the largest electricity storage unit, which can also improve electrical energy quality. Therefore, PSPS has been widely built during the past decades [1], [3]

To ensure the flexibility and stability of modern grids, it is crucial to enhance and sustain the reliability of hydropower stations, particularly Pumped Storage Power Stations (PSPSs) [4]. The key to achieving optimal reliability lies in analyzing the root causes of common faults and subsequently avoiding these faults or implementing early warning systems for these faults.

The associate editor coordinating the review of this manuscript and approving it for publication was Paolo Giangrande.

Hydro-generators consist of multiple windings connected by lead wires, which are consistently subjected to high stress, making fatigue fractures of these lead wires common. This is especially true for hydro-generators in PSPSs, as they experience more frequent starts and stops, resulting in greater stress [5]. PSPSs also have unique operational modes, including peak-valley filling, frequency and phase modulation, and rapid response functions like spinning reserve. Consequently, during PSPS operation, large-scale load changes often occur, increasing lead wire stress [6]. This makes hydro-generators in PSPSs more susceptible to fatigue fractures in rotor winding lead wires, causing damage to generator components, grid instability, and even significant economic or social losses.

To address this fault, a proposed approach involves optimizing the local geometry of the lead wire to alleviate stress concentration and reduce local maximum stress. For instance, Di [7] conducted an analysis on the mechanical and thermal stress of the lead wire with various structures and suggested modifying the key radius as a means to decrease maximum stress. However, it should be noted that this method primarily extends the fatigue life of the lead wire but does not entirely

prevent fractures or the subsequent losses associated with them. Due to the inherent fatigue life of any material, it is not feasible to completely avoid fatigue fractures in lead wires. As a result, ensuring the high reliability of the lead wire heavily relies on early warning systems for this particular fatigue fracture.

Fault early warning systems have found wide application in various fields such as finance [8], medicine [9], and geological disaster forecasting [10]. Their primary purpose is to mitigate potential risks, eliminate hidden hazards, and enhance the overall reliability of the system by issuing alarm signals prior to the occurrence of faults. In the case of lead wire fatigue fractures, two approaches can be employed for early warning. The first approach involves triggering an alarm signal before the lead wire completely breaks. The second approach entails introducing a redundant lead wire into the existing system and issuing an alarm signal when the original lead wire fails while the redundant one remains intact. Redundancy, which involves duplicating certain components within a system, is a widely employed concept across various domains [11], [12], [13]. In this paper, the redundant lead wire is introduced by replacing the original single lead wire with a dual-connection lead wire, both serving the same function. Consequently, if a fault occurs in the original lead wire during generator operation, the redundant lead wire ensures the normal functioning of the generator. It is worth noting that the first approach is more challenging to implement as it requires accurate prediction of the fatigue life of the lead wire. In contrast, the second approach only requires a rough estimation of the difference in fatigue life between the two lead wires to have sufficient reliability. Because, as long as the redundant lead wire's fatigue life is significantly longer than that of the original lead wire, maintenance personnel will have ample time to update the damaged lead wire before the redundant one fractures, even if the length of this time is inaccurately estimated (which can be calculated from the estimated difference in fatigue life between the two lead wires).

Fault early warning requires a reliable fracture monitoring system for detecting faults and promptly sending alarm signals, which can be achieved using optical fiber [14], acoustic emission [15], or temperature change detection [16]. This paper employs a resistance change-based fracture monitoring mechanism to enhance the real-time performance. Integrating this real-time fracture monitoring system with dual-connection lead wires allows for early fatigue fracture warnings in lead wires of the rotor winding. Upon receiving an alarm signal, maintenance personnel can take swift action to minimize or even eliminate losses resulting from fatigue fractures.

This paper proposes a highly reliable hydro-generator rotor winding lead wire scheme in PSPS, featuring early warning for fatigue fractures. The scheme includes dual-connection lead wires and a real-time fracture monitoring system. The paper also validates the scheme's reliability and practicality through testing and theoretical analysis. The remainder is organized as follows: Section II details the early warning implementation; Section III describes the fatigue testing machine's mechanism and structure, including a real-time fracture monitoring system; Section IV discusses the machine's validity test results; Section V presents a theoretical analysis based on the P-S-N fatigue life prediction model; and Section VI concludes the paper.

II. INPLEMENTATION OF FAULT EARLY WARNING SYSTEM

Fig. 1 shows that generators in pumped storage power stations frequently start or stop, resulting in greater dragging force on the lead wires between adjacent rotor windings compared to those in ordinary hydro-generators. This force often leads to lead wire fractures and serious consequences. To address this issue, this paper proposes a new fault early warning scheme that incorporates a dual-connection lead wire and a real-time fracture monitoring system. The dual-connection lead wire system adds a redundant lead wire, which is connected in parallel to the original lead wire. These two lead wires have different structural characteristics and, consequently, different fatigue lives under the same displacement amplitude along the dragging force direction. This ensures that the redundant lead wire can sustain the operation of generators and their rotors for a certain period after the original lead wire ruptures. Therefore, as long as maintenance personnel repair or replace the broken lead wire before the redundant lead wire ruptures, the generator and its rotor can continue to function under normal conditions.

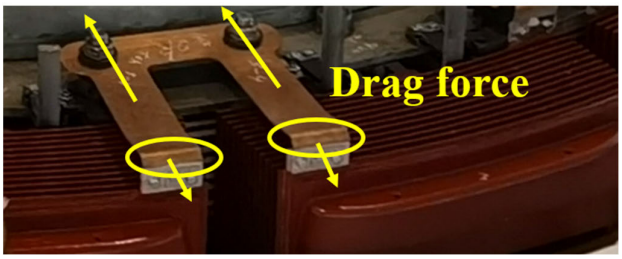

FIGURE 1. Structure of the lead wire between rotor windings.

By integrating the dual-connection lead wire with a real-time fracture monitoring system, the detection of fatigue fractures in the original lead wire allows for complete fault early warning. The alarm signal from the early warning system can then be utilized by maintenance personnel to plan for generator shutdown. The monitoring system operates on a six-resistance mechanism, as depicted in Fig. 2. The equivalent circuit of the dual-connection lead wire consists of two parallel branches, with each branch representing a lead wire containing three equivalent resistances. The contact resistances between the original wire or redundant wire and rotor windings are denoted by R_1, R_4, R_2, and R_3. Additionally, the two lead wires possess their own connecting resistances, denoted by R_{14} and R_{23}.

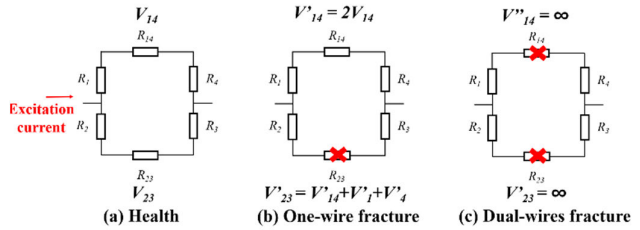

FIGURE 2. Equivalent circuit under (a) health, (b) one-wire fracture and (c) double-wires fracture condition.

Fractures can be detected by monitoring the voltage drops across these resistances under excitation current (can be regarded as the constant current condition). When both lead wires are intact, the current is divided between the two branches in proportion to the ratio of $(R_1 + R_{14} + R_4)$ and $(R_2 + R_{23} + R_3)$. In the case of the dual-connection lead wire, the resistance values of the two branches are nearly equal, resulting in a similar flow of current through both branches. Consequently, $V_{14} \approx V_{23}$. However, if the lead wire with R_{23} breaks, the current will solely flow through the redundant wire with R_{14}, leading to a voltage drop on R_{14}, denoted as V'_{14}, that is nearly twice the healthy voltage drop V_{14}. The voltage drop on R_{23}, denoted as V'_{23}, is approximately equal to the sum of V'_{14}, V'_1, and V'_4. In the event that both lead wires are broken, the voltage drops on R_{14} and R_{23} tend towards infinity. Therefore, the fracture of the lead wire can be detected by monitoring the changes in V_{14} and V_{23}.

In conclusion, the combination of the real-time fracture monitoring system and the dual-connection lead wire provides an effective and reliable early warning system for lead wire fractures. However, the practicality and feasibility of this scheme need to be verified through validity tests and theoretical analysis.

III. FABRICATION OF THE FATIGUE TESTING MACHINE

The testing machine has two essential functions: simulating the fatigue process of lead wire, and diagnosing the first wire's fracture by monitoring the lead wire's resistance. As shown in Fig. 3(a), the testing machine consists of three parts: the mechanical transmission system, the constant current system, and the fracture monitoring system.

The overall operating mechanism of the fatigue testing machine shows in Fig. 3(b). Mechanical transmission system transforms the fixed-axis rotation into a cyclic dragging motion. The constant current source provides a stable current (used to simulate the excitation current on the rotor windings) for dual-connection lead wire. The fracture monitoring system extracts voltage signals from the lead wires of the lead wire using signal probes, then amplifies these signals through a differential amplification module, and uploads them to a PC for subsequent analysis via an A/D converter.

The structure of dual-connection lead wire on the testing machine is shown in Fig. 4. This structure has two single wires with different structural characteristics. Each wire has two head segments and a middle segment. Head segments

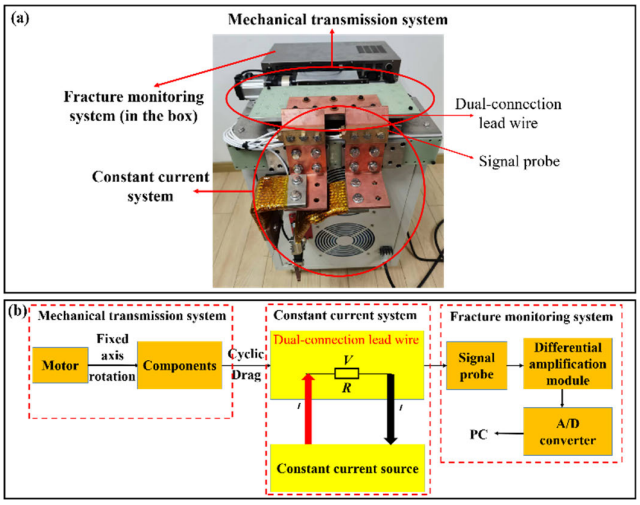

FIGURE 3. (a) Physical composition and (b) overall mechanism of fatigue testing machine.

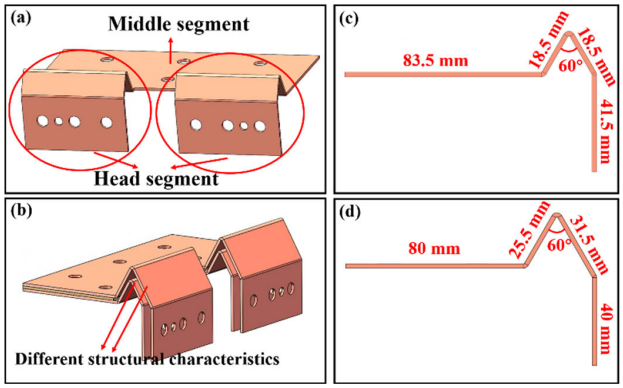

FIGURE 4. The structure and size of the dual-connection lead wire used in validity test.

provide sites for probes to extract voltage signals for fracture monitoring. The Middle segment is fixed with the slide platform of the testing machine to simulate the fatigue process. The special corner between the head segment and the middle segment is the area of most apparent stress concentration, and thus, it is always the fracture position. Besides, this corner could reduce the time to wire's fracture and speed up the testing process.

The fracture monitoring system consists of signal probes and a signal processing circuit. Signal probes extract voltage signals from dual-connection lead wire under the constant current condition. Signals are analyzed by the processing circuit and final results will be transmitted to the upper computer. Four signal probes are installed on four head segments of lead through bolts, as shown in Fig. 5(a). There are four contact resistances between wire's head segment and input or output plates as well as two connecting resistances whose voltage drops are extracted by signal probes. There are two thimbles inside the probe to directly contact test sites. The short thimble contacts the head segment as one site. The long thimble passes through the hole on the head segment and

reaches the input or output plate as the other site, as shown in Fig. 5(b).

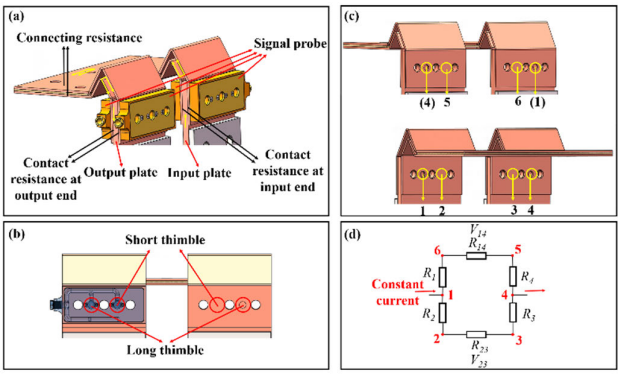

FIGURE 5. (a) Installation and (b) structure of signal probes; mapping of extracting sites on (c) the real lead wire and (d) the equivalent circuit.

Therefore, four probes could extract eight voltage signals from 8 test sites as shown in Fig. 5(c). Because the input or output plate is approximated as ideal conductor, No. (1) and No. (4) sites are equivalent to No.1 and No.4 sites, respectively. Voltage drops between every two sites reflect the change in six resistances under constant current conditions, as shown in Fig. 5(d). Signal probes extract six voltage signals from six sites and transmit them to the subsequent processing circuit, and then the voltage drops in Fig. 5(d) are analyzed by the processing circuit. $V_1 \sim V_4$ represent the voltage drops on $R_1 \sim R_4$, V_{14} and V_{23} represent the voltage drops on R_{14} and R_{23}. The key module used to calculate the voltage drops in the processing circuit is mainly based on the analog subtractor that has 30 times amplification gain.

Validity test for dual-connection lead was conducted using the above testing machine. The structure of the lead wire used in test is shown in Fig. 4. The test parameters are set as shown in table 1.

TABLE 1. Parameter setting of the validity test.

Parameters	Value
Motor's rotation speed	600 r/min
Reduction ratio	10:1
Voltage signal's extracting frequency	10 Hz
Constant current source	1000 A/ 0.5 V output limit
Material of sample	T2 pure copper

IV. VALIDITY TEST RESULTS OF DUAL-CONNECTION LEAD WIRE ON THE FATIGUE TESTING MACHINE

V_{23} and V_{14} (before $\times 30$) are acquired from the validity test, as shown in Fig. 6. According to Fig. 6(a), the fatigue process of the lead wire has three periods. During the second and the third period, there are obvious oscillations that are caused by periodic contact and separation of the ruptured wire.

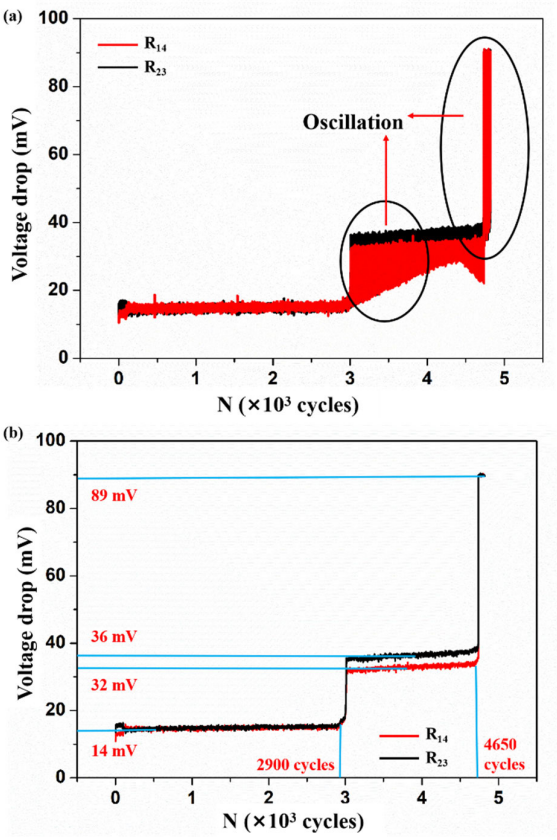

FIGURE 6. V_{23} and V_{14} of the validity test on testing machine.

Fig. 6(b) only shows the maximum amplitude per cycle that reflects the value of V_{23} and V_{14} when two lead wires are separated. Therefore, the following analysis is based on Fig. 6(b). The first period goes through ~2900 cycles from the start of the validity test to the fracture of the original lead wire. During this period, neither of the two lead wires were broken, so the voltage drops V_{23} & V_{14} are equal and their values are ~14mV. The second period goes through ~1750 cycles (=4650-2900) until the fracture of the redundant lead wire. During this period, only the original wire was broken, so the V_{23} & V_{14} become about twice their original value and the V_{23} is slightly larger than the V_{14}. During the third period, both of two lead wires were broken, so the V_{23}& V_{14} reach the smaller output limit of processing circuit (2.7 V≈89 mV×30) and constant current source (0.5 V=15 V÷30). The same test is repeated two more times, the first period goes through 2750 cycles or 3100 cycles, and the second period goes through 1500 cycles or 2060 cycles, respectively. These results preliminarily proves that the dual-connection lead wire system has prominent redundant time and the real-time fracture monitoring system is effective.

V. ANALYSIS BASED ON THE P-S-N LIFE PREDICTION MODEL

The fatigue test on the testing machine only preliminarily proves that the dual-connection lead wire system has prominent redundant time. Only when the redundant time could be

easily predicted and adjusted, the method combining the dual-connection lead wire and the real-time fracture monitoring system is really reliable and practical. *P-S-N* life prediction model based on Weibull distribution could achieve the above goal. The data required to fit the parameters in this model could be obtained through the standard fatigue test. The detailed process of the standard fatigue test sees the appendix. The fitted parameters of this model are shown in table 2. Substituting these parameters into the *P-S-N* model could obtain quantitative functional form of this model, which is denoted as *PSN*.

Using the *P-S-N* model could obtain the *S-N* curve of the lead wire under different *P*, as shown in Fig. 7. It is discovered that the wire has shorter fatigue life under larger stress. Greater endurable failure probability *P* corresponds to a longer expected fatigue life and vice versa. With the help of the *P-S-N* model, the universality of the redundant time of the dual-connection lead wire could be proved theoretically and this redundant time could be estimated reliably.

TABLE 2. Parameters of single wire's weibull distribution model.

A	*B*	*μ*	*a*	*b*	*c*
0.855	2.213	1.22	1.195	0.015	1.055

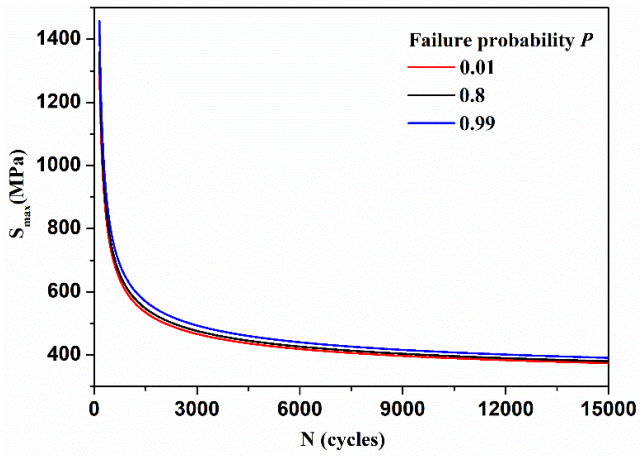

FIGURE 7. *S-N* curve of the single wire obtained using parameters (table 2).

Table 3 and table 4 show the results of the finite element simulation on the dual-connection lead wire in Fig. 4. And two wires' stress concentration conversion factors (the detailed definition sees in appendix B) are ∼0.07830% and ∼0.1220%, which could be obtained using linear regression from the results in Table 3 and 4.

According to equation (S1), the relationship between the two wires' ratio of S_{max} and k is shown in equation (1) under equal amplitude of displacement

$$\frac{S'_{\max}}{S_{\max}} = \frac{k}{k'} \tag{1}$$

TABLE 3. Results of finite element simulating on the first wire of dual-connection lead.

D (mm)	Nominal S_{max} (MPa)	$k=D/S_{max}$
1	1277	0.07831%
0.9	1150	0.07826%
0.8	1022	0.07828%
0.7	894	0.07830%
0.6	766	0.07833%
0.5	639	0.07825%

TABLE 4. Results of finite element simulating on the redundant wire of dual-connection lead wire.

D (mm)	Nominal S_{max} (MPa)	$k=D/S_{max}$
1	820	0.12195%
0.9	738	0.12195%
0.8	656	0.12195%
0.7	574	0.12195%
0.6	492	0.12195%
0.5	410	0.12195%

where S_{max} and S_{max}' are the nominal stresses of the original wire and the redundant wire, respectively. For the dual-connection lead wire used in the validity test, the stress ratio γ (= S_{max}'/S_{max}) is 0.642.

Substituting the stress ratio into equation (S1), the relationship between S_{max} and the displacement amplitude D of these two wires could be derived, as shown in equation (2).

$$S'_{\max} = S_{\max} \cdot \gamma = \frac{D}{k} \cdot \gamma \tag{2}$$

Substituting the equation (2) into the *P-N-S* model, the fatigue life of the original wire N, the fatigue life of the redundant wire N', and the relationship between their difference $\Delta N = N'\text{-}N$ and D could be obtained, as shown in equation (3).

$$\begin{aligned}\Delta N = N' - N &= \mathrm{PSN_{P'}}(S') - \mathrm{PSN_P}(S) \\ &= \mathrm{PSN_{P'}}(\frac{D}{k} \cdot \gamma) - \mathrm{PSN_P}(\frac{D}{k})\end{aligned} \tag{3}$$

where $\mathrm{PSN_P}$ and $\mathrm{PSN_{P'}}$ represent *PSN* function with specific value of P or P'. According to the equation (3), the redundant time could be predicted given that D, k, and γ are known. Taking the dual-connection lead wire in Fig. 4 as an example, its γ and k are 0.642 and 0.000783, respectively. Then, Quantitative relationship between ΔN and D could be derived from equation (3), if P and P' are set as 0.99 and 0.01, respectively, as shown in Fig. 8. (Curve in Fig. 8 uses the logarithmic ordinate).

According to Fig. 8, it can be observed that ΔN increases continuously as D decreases. Therefore, the dual-connection lead wire can be considered reliable, as long as ΔN, corresponding to the maximum possible value of displacement amplitude $D_{\max}$, meets the actual requirement.

However, the lead wire's fatigue process is the result of the combination of many different displacement amplitudes. Therefore, it is necessary to analyze the redundant time under the multiple displacement amplitude and compare it with the analysis under the single displacement amplitude.

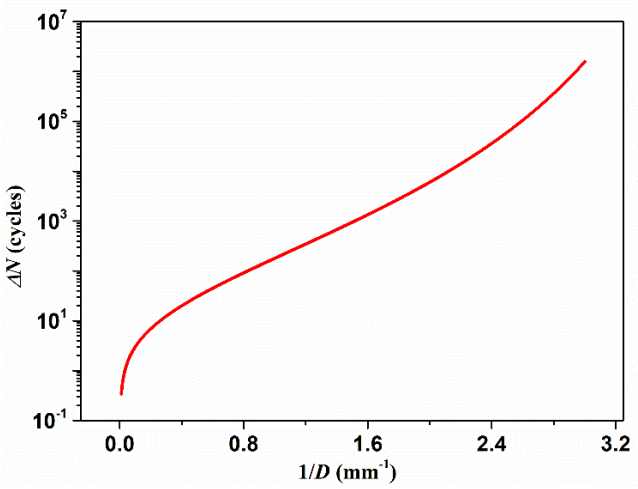

FIGURE 8. Relationship between ΔN and the $1/D$.

Suppose that the dual-connection lead wire is affected by two amplitudes of displacement D_1 and D_2 ($D_1 > D_2$). The fatigue lifetimes of the first wire under these two amplitudes of displacement are N_1 and N_2 that are determined by D_1 and D_2. The fatigue lifetimes of the redundant wire are N_1' and N_2', respectively. Then, the fatigue damage per cycle of the first wire under these two amplitudes of displacement are i_1 and i_2 that are defined as equation (4) and (5). The fatigue damages per cycle of the redundant wire under two amplitudes of displacement are i_1' and i_2' that are defined as equation (6) and (7).

$$i_1 = \frac{1}{N_1} \tag{4}$$

$$i_2 = \frac{1}{N_2} \tag{5}$$

$$i_1' = \frac{1}{N_1'} \tag{6}$$

$$i_2' = \frac{1}{N_2'} \tag{7}$$

During a period of time, the cycles of D_1 and D_2 are n_1 and n_2, respectively. Then, the cumulative damage of the first wire is I that are defined as equation (8). Because two wires are affected by equal amplitude of displacement at any time,

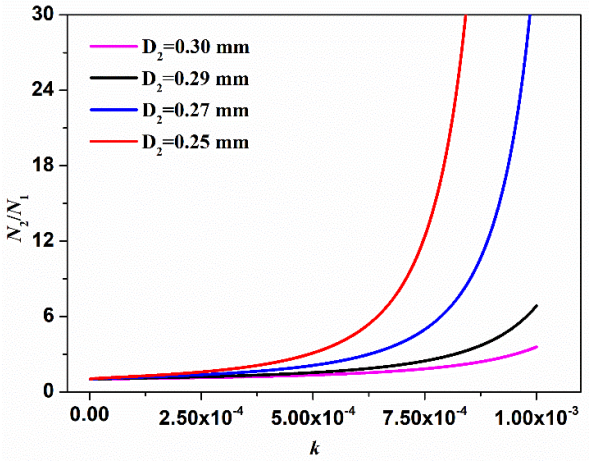

FIGURE 9. Relationship between the cumulative damage of the redundant wire I' and load cycles of the first amplitude of displacement.

the cumulative damage of the redundant wire is I' that are defined as equation (9).

$$I = n_1 i_1 + n_2 i_2 = \frac{n_1}{N_1} + \frac{n_2}{N_2} \tag{8}$$

$$I' = n_1 i_1' + n_2 i_2' = \frac{n_1}{N_1'} + \frac{n_2}{N_2'} \tag{9}$$

Suppose that the first wire has ruptured, which means I is equal to 1. This condition brings a quantitative relationship between n_2 and n_1, which means n_2 could be expressed by n_1. According to P-S-N model and equation (2), N_1' and N_2' are also determined by D_1 and D_2, respectively. Therefore, if the P, D_1 and D_2 is given, the N_1, N_2, N_1', N_2' could be calculated using the P-S-N model and equations (16-21). Then, I' could be simplified as the function of n_1, as shown in equation (10). Because both n_1 and n_2 must be greater than zero and $I = 1$, the valid domain of n_1 is between 0 to N_1.

$$I'(n_1) = \left(\frac{1}{N_1'} - \frac{N_2}{N_1 N_2'}\right) \times n_1 + \frac{N_2}{N_2'} \tag{10}$$

$$\frac{N_2'}{N_1'} > \frac{N_2}{N_1} \tag{11}$$

$$\frac{1}{N_1'} - \frac{N_2}{N_1 N_2'} > 0 \tag{12}$$

As depicted in Fig. 9, the ratio between a lead wire's fatigue life under the individual influence of two displacement amplitudes and the lead wire's k value exhibits a monotonically increasing relationship. In other words, a larger k value results in a larger N_2/N_1 ratio. Consequently, equation (11) always holds true due to the fact that k' is greater than k, as explained previously. Then, equation (12) also always holds true as equation (11) and equation (12) are equivalent. Hence, it can be proven that $I'(n_1)$ is an always-monotonically increasing linear function, implying that I' reaches its maximum value only when $n_1 = N_1$ (the valid domain of n_1 is $[0, N_1]$). This condition is corresponding to the individual action of D_1 (the larger displacement amplitude). Therefore, when the fracture

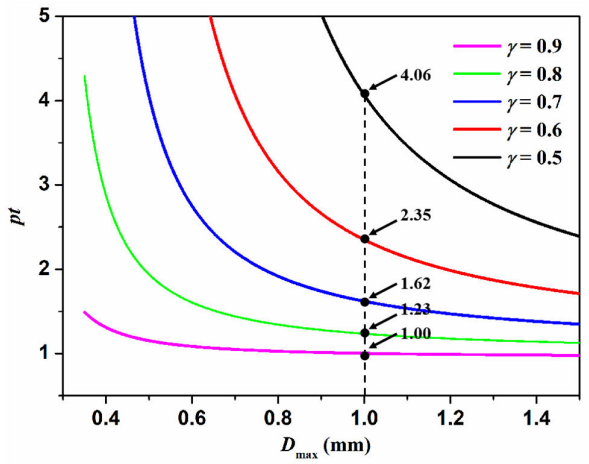

FIGURE 10. Relationship between *pt* and D_{max} under different γ (P=0.99 P'=0.01).

of the original lead wire may be the result of the combined effect of two different displacement amplitudes, the scenario with the individual larger displacement amplitude yields the highest estimation of cumulative damage for the redundant lead wire. This estimation aligns with the most conservative assessment of the redundant lead wire's fatigue life. In conclusion, utilizing the individual larger displacement amplitude instead of the combination effect of two displacement amplitudes provides a more reliable prediction of the redundant lead wire's fatigue life.

The above conclusion can be naturally extended to scenarios with multiple displacement amplitudes. Hence, it is sufficiently reliable to predict the fatigue life of the redundant wire under the single D_{max}, given the fatigue life of the original lead wire. Furthermore, estimating or predicting ΔN and other related parameters under the single D_{max} is also considered reliable.

To facilitate understanding for maintenance personnel, the correlation between the fracture time ratio of two lead wires and D_{max} is derived from the ΔN-D relationship. The fracture time of the original wire is denoted as t, while the fracture time of the redundant wire is denoted as t'. Both t and t' are subject to the relationships specified in equations (13) and (14).

$$t = \frac{N}{f} \tag{13}$$

$$t' = \frac{N'}{f} \tag{14}$$

where f is the frequency of the amplitude of displacement. The fracture time ratio is $pt = t'/t$, which is depicted by equation (15).

$$pt = \frac{t'}{t} = \frac{N'}{N} \tag{15}$$

The functional relationship between pt and D_{max} can be derived using the P-S-N model, as depicted in Fig. 10. This curve enables the estimation of the fracture time ratio when the maximum displacement amplitude D_{max} and the stress ratio of the two lead wires are known. For instance, if D_{max} is 1 mm and γ is 0.8, the fracture time ratio is estimated to be 1.22. By utilizing pt, the redundant time of the redundant lead wire can be further estimated when the fracture time of the original lead wire is obtained through the fracture monitoring system.

In practical scenarios, even if the original lead wire has ruptured, it is not permissible to immediately shut down the faulty generator due to its vital role in the power station. Therefore, the estimation of redundant time becomes crucial as it provides maintenance personnel with the latest downtime of the faulty generator, enabling them to schedule specific downtime according to the actual demand. Furthermore, if the redundant time falls short of meeting the actual demand, adjustments can be made to γ by modifying the structure of the redundant lead wire and subsequently adjusting pt until the actual demand is met.

The fracture time of the original lead wire is nearly 10 years (e.g. 7 years in Heimifeng power station of China) Even when γ is set to 0.8, the redundant time should be more than 1 year (D_{max} =1mm), which exceeds the actual requirement. Hence, a value of 0.8 is sufficient for γ in lead wire design. This value is close to 1, making it easily attainable during the design of the redundant lead wire. Consequently, the early warning scheme is deemed practical.

VI. CONCLUSION

A new scheme integrating the dual-connection lead wire and the real-time fracture monitoring system is proposed to realize early warning for the fatigue fracture. The reliability and practicality of this scheme is proved through testing and theoretical analysis:

(1) The validity test on the testing machine proves that the real-time fracture monitoring system based on the six-resistance monitoring mechanism could detect the fracture timely and accurately.

(2) The functional relationship between ΔN and D, established based on the P-S-N life prediction model, can quantitatively predict the ΔN of the dual-connection lead wire when D is known. Moreover, if the known D is the global maximum value D_{max}, then the prediction of ΔN and its derivatives is sufficiently reliable in practical situations (where the lead wire is subjected to multiple displacement amplitudes).

(3) The pt-D_{max} relationship derived from the ΔN-D relationship can predict the redundant time of dual-connected leads under the condition of known D_{max} and the fracture time of the original lead wire, providing maintenance personnel with a reference value for the latest shutdown time. In addition, this relationship can also guide lead wire designers to quantitatively adjust the expected redundant time by changing the lead wire's structure under the condition of known D_{max}.

In summary, the fault early warning system, which integrates dual-connection lead wires, the real-time fracture monitoring, and redundant time estimation based on the *P-S-N* fatigue life prediction model, demonstrates strong practicality and fundamentally enhances the reliability of rotor winding's lead wires in PSPSs.

APPENDIX
THE CONSTRUCTION OF THE P-S-N FATIGUE LIFE PREDICTION MODEL OF THE SINGLE WIRE

The process of the establishment consists of two steps. The first step is to conduct the standard fatigue test on a single wire whose material is the same as the dual-connection lead wire. Their structures should have similar special corners. The second step is to fit parameters in the *P-S-N* model using the results of the standard fatigue test.

A. STRUCTURE OF THE SINGLE WIRE

The structure of the single wire used in the standard fatigue test omits the intermediate segment and head segments. It only has the special corner that has the most apparent stress concentration, as shown in Fig. 11(b). The size parameters are shown in Fig. 11(a).

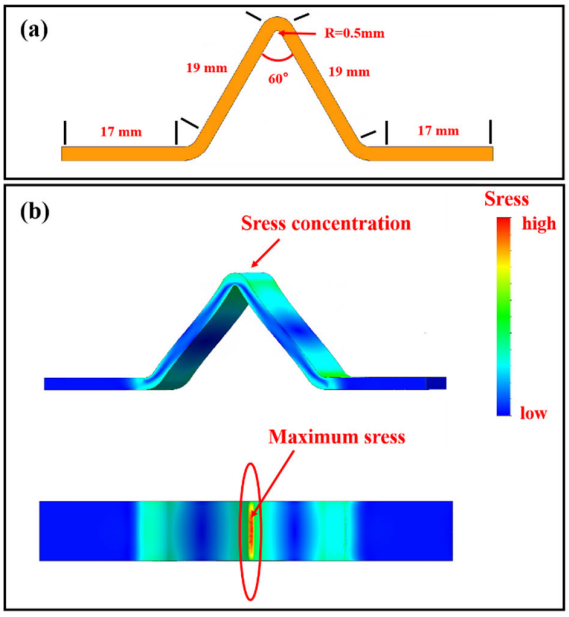

FIGURE 11. (a) Structure and (b) stress distribution of single wire using in standard fatigue test.

B. NOMINAL STRESS OF THE SINGLE WIRE

In Fig. 11(b), the maximum stress S_{max} is located in the area adjacent special corner. This stress is regarded as nominal stress, to replace the complex stress distribution on the single wire. There is a fixed proportional relationship between S_{max} and the amplitude of displacement D on this single wire, as shown in equation (S1).

$$D = kS_{\max} \tag{S1}$$

k is defined as the stress concentration conversion factor representing the wire's stress distribution. It could be obtained using a finite element simulation.

C. PARAMETER SETTING IN THE STANDARD FATIGUE TEST

The standard fatigue test is conducted on this single wire. In the test, the amplitude of displacement imposed to the wire is constant. Detailed parameter settings are shown in table 5.

TABLE 5. Parameter settings of the standard fatigue test.

Parameters	Value
Equipment	Walter-bai fatigue testing machine
Stress ratio	-1
Load frequency	5Hz
Load type	Constant amplitude of displacement
Material of sample	T2 pure copper

D. RESULTS OF THE STANDARD FATIGUE TEST

The standard fatigue test chooses four amplitudes of displacement and sets five parallel samples for each amplitude of displacement. The nominal S_{max} and the test results under different amplitudes of displacement show in table 6.

TABLE 6. Results of standard fatigue test for single wire.

Amplitude of displacement (mm)	Nominal S_{max} (MPa)	Fatigue lifetime (cycles)
0.35	447	3969, 4285, 4562, 3722
0.33	422	9710, 5555, 5683, 8667
0.3	383	12999, 11863, 16512, 12544
0.25	319	127169, 116634, 102572, 110869

E. P-S-N LIFE PREDICTION MODEL BASED ON THE WEIBULL DISTRIBUTION

Lifetime prediction model could be obtained using the results in table 6. The primary fatigue life prediction model depicted by *S-N* curve is Basquin (1910) model, as shown in equation (S2).

$$Log\left(N_f\right) = A - B\log\left(\sigma\right) \tag{S2}$$

But this model only considers physical arguments and omits the distribution of fatigue test results [17], [18]. Therefore, it is impossible to ensure high reliability of design. Besides, this model needs lots of samples to fit so that it is not practical. Some other models could also be used to depict the relationship between the fatigue life N and the stress range S.

The three-parameter Weibull model, $W(a, b, c)$, could take the probability distribution of fatigue test results into account and it has high goodness of fit even using few samples.

The cumulative distribution failure function (CDF, also called failure distribution or life distribution) of Weibull model for the random variable x is shown in equation (S3).

$$P(x|a,b,c) = 1 - \exp(-(\frac{x-a}{b})^c), \text{ x} \geq \text{a} \tag{S3}$$

where a represents location parameter, b represents scale parameter, c represents shape parameter [19]. In the case of fatigue modelling, Castillo et al. consider that the conditional CDF of the random variables lifetime and stress are not independent and must satisfy a compatibility condition which leads to a functional equation. The solution of this functional equation leads to a probabilistic fatigue model for a constant stress, which is based on a Weibull distribution [20], as shown in equation (S4), where the random variable is shown in equation (S5)

$$\begin{aligned} &P(N,S|A,B,a,b,c) \\ &\quad = 1 - \exp(-(\frac{(\log N - A)(\log S - B) - a}{b})^c) \qquad \text{(S4)} \\ &x = (\log N - A)(\log S - B) \qquad \text{(S5)} \end{aligned}$$

where N represents the number of load cycles up to failure, S represents the stress range, A, B, a, b, c and μ are parameters need to be fitted.

1) PARAMETER ESTIMATION

Supposing that n stress ranges and the average of corresponding load cycles are given as equation (S6).

$$\begin{aligned} &N_1, N_2, , N_n \\ &S_1, S_2, , S_n \end{aligned} \tag{S6}$$

A, B and μ of probabilistic fatigue model are estimated by solving the following non-linear optimization problem [21].

$$R = \sum_{i=1}^{n} (\log N_i - A - \frac{\mu}{\log S_i - B})^2 \tag{S7}$$

Parameters, a, b, and c could be estimated using probabilistic weighted matrix (PWM) method. The PWMs of a random variable x with CDF is shown in equation (S8).

$$M_{p,r,s} = \int_0^1 x(P)^p * P^r * (1-P)^s dP \tag{S8}$$

In this paper, only elements with p, r and s as specific values are used, such as $M_{1,0,0}$, $M_{1,0,1}$, $M_{1,0,2}$. Their deduction and properties from a Weibull distribution are presented in equation set (S9).

$$\begin{aligned} M_{1,0,0} &= a + b \cdot \Gamma(1 + \frac{1}{c}) \\ M_{1,0,1} &= \frac{a}{2} + \frac{b}{2^{1+\frac{1}{c}}} \cdot \Gamma(1 + \frac{1}{c}) \\ M_{1,0,2} &= \frac{a}{3} + \frac{b}{3^{1+\frac{1}{c}}} \cdot \Gamma(1 + \frac{1}{c}) \end{aligned} \tag{S9}$$

Solving this equation set leads to the equations for calculating a, b and c, as shown in equation (S10)∼S12).

$$\frac{3M_{1,0,2} - M_{1,0,0}}{2M_{1,0,1} - M_{1,0,0}} = \frac{3^{-\frac{1}{c}} - 1}{2^{-\frac{1}{c}} - 1} \tag{S10}$$

$$b = \frac{2M_{1,0,1} - M_{1,0,0}}{(2^{-\frac{1}{c}} - 1) \cdot \Gamma_c} \tag{S11}$$

$$a = M_{1,0,0} - b \cdot \Gamma_c \tag{S12}$$

The value of $M_{1,0,0}$, $M_{1,0,1}$, $M_{1,0,2}$ could be calculated by equation (S13).

$$\begin{cases} M_{1,0,0} = \dfrac{1}{n} \displaystyle\sum_{i=1}^{n} x_i, \\ M_{1,0,1} = \dfrac{1}{n(n-1)} \displaystyle\sum_{i=1}^{n} (i-1)x_i, \\ M_{1,0,2} = \dfrac{1}{n(n-1)(n-2)} \displaystyle\sum_{i=1}^{n} (i-1)(i-2)x_i \end{cases} \tag{S13}$$

REFERENCES

[1] A. Tuohy and M. O'Malley, "Pumped storage in systems with very high wind penetration," *Energy Policy*, vol. 39, no. 4, pp. 1965–1974, Apr. 2011.
[2] L. Yuan, J. Zhou, C. Chang, P. Lu, C. Wang, and M. Tayyab, "Short-term joint optimization of cascade hydropower stations on daily power load curve," in *Proc. IEEE Int. Conf. Knowl. Eng. Appl. (ICKEA)*, Sep. 2016, pp. 236–240.
[3] Y. X. He, L. Guan, Q. Cai, X. L. Liu, and C. R. Li, "Analysis of securing function and economic benefit of pumped storage station in power grid," *Power Syst. Technol.*, vol. 28, pp. 54–57, Jan. 2004.
[4] A. Golshani, W. Sun, Q. Zhou, Q. P. Zheng, J. Wang, and F. Qiu, "Coordination of wind farm and pumped-storage hydro for a self-healing power grid," *IEEE Trans. Sustain. Energy*, vol. 9, no. 4, pp. 1910–1920, Oct. 2018.
[5] P. J. Donalek, "Pumped storage hydro," *IEEE Power Energy Mag.*, vol. 18, no. 5, pp. 49–57, Sep. 2020.
[6] C. Liu, J. Zhou, X. Lai, and T. Zhang, "Optimization and mechanism of the wicket gate closing law for high-head pumped storage power stations," *IEEE Access*, vol. 9, pp. 11734–11749, 2021.
[7] H. Di, G. Hao, Z. Zhang, J. Chen, Z. Hou, H. Di, B. Yang, Y. Mo, Y. Chen, and K. Hu, "Three-dimensional stress analysis of generator-motor pole-lead with different structures," in *Proc. IEEE 3rd Int. Electr. Energy Conf. (CIEEC)*, Sep. 2019, pp. 1986–1990.
[8] Y. Liang, D. Quan, F. Wang, X. Jia, M. Li, and T. Li, "Financial big data analysis and early warning platform: A case study," *IEEE Access*, vol. 8, pp. 36515–36526, 2020.
[9] F. E. Shamout, T. Zhu, P. Sharma, P. J. Watkinson, and D. A. Clifton, "Deep interpretable early warning system for the detection of clinical deterioration," *IEEE J. Biomed. Health Informat.*, vol. 24, no. 2, pp. 437–446, Feb. 2020.
[10] Y. Zhanying, Z. Yupeng, L. Bing, M. Xifeng, Z. Xu, M. Yue, G. Shuangtian, and K. Xiaoang, "Surface deformation monitoring and identification of potential geological hazards in funing pumped storage power station based on time series InSAR," in *Proc. IEEE 5th Adv. Inf. Manage., Communicates, Electron. Autom. Control Conf. (IMCEC)*, vol. 5, Dec. 2022, pp. 1807–1813.
[11] Y. Jiang, Y. Wang, and Z. Zhang, "Design of multistage evolution of different-structure redundant digital system based on graph theory," in *Proc. Int. Conf. Electr. Inf. Control Eng.*, Apr. 2011, pp. 4117–4120.
[12] P. K. Kapur and K. R. Kapoor, "Stochastic behaviour of some 2-unit redundant systems," *IEEE Trans. Rel.*, vol. R-27, no. 5, pp. 382–385, Dec. 1978.
[13] A. D. Narasimhalu and H. Sivaramakrishnan, "A rapid algorithm for reliability optimisation of parallel redundant systems," *IEEE Trans. Rel.*, vol. R-27, no. 4, pp. 261–263, Oct. 1978.

[14] H. Cao, Y. Hao, Z. Zhang, J. Wei, and L. Yang, "System and method of quasi-distributed fiber Bragg gratings monitoring brittle fracture process of composite insulators," *IEEE Trans. Instrum. Meas.*, vol. 70, pp. 1–10, 2021.
[15] M. D. Prieto, D. Z. Millan, W. Wang, A. M. Ortiz, J. A. O. Redondo, and L. R. Martinez, "Self-powered wireless sensor applied to gear diagnosis based on acoustic emission," *IEEE Trans. Instrum. Meas.*, vol. 65, no. 1, pp. 15–24, Jan. 2016.
[16] C. Li, Z. Ma, W. Zhang, S. Tong, S. Wang, H. Zhao, and L. Ren, "Realization of tensile-bending mechanical-thermal coupling fatigue based on a uniaxial tensile-fatigue testing device," *IEEE Trans. Instrum. Meas.*, vol. 71, pp. 1–9, 2022.
[17] K. N. Meyyappan, P. Hansen, and P. McCluskey, "Wire fatigue model for power electronic modules," in *Proc. ASME Int. Mech. Eng. Congr.*, Washington, DC, USA, 2003, pp. 257–265.
[18] H. L. J. Pang, T. L. Tan, J. F. Leonard, and Y. S. Chen, "Reliability assessment of a wirebond chip-on-board package subjected to accelerated thermal cycling loading," in *Proc. 1st Electron. Packag. Technol. Conf.*, Singapore, 1997, pp. 93–97.
[19] P. D. Toasa Caiza and T. Ummenhofer, "General probability weighted moments for the three-parameter Weibull distribution and their application in S–N curves modelling," *Int. J. Fatigue*, vol. 33, no. 12, pp. 1533–1538, Dec. 2011.
[20] E. Castillo and J. Galambos, "Lifetime regression models based on a functional equation of physical nature," *J. Appl. Probab.*, vol. 24, no. 1, pp. 160–169, Mar. 1987.
[21] J. A. F. O. Correia, P. J. Huffman, A. M. P. De Jesus, S. Cicero, A. Fernández-Canteli, F. Berto, and G. Glinka, "Unified two-stage fatigue methodology based on a probabilistic damage model applied to structural details," *Theor. Appl. Fract. Mech.*, vol. 92, pp. 252–265, Dec. 2017.

YUNHAN ZHANG was born in Shandong, China, in July 1997. He received the B.E. degree in composite material and engineering from the Northwestern Polytechnical University, Xi'an, China, in 2016. Now he is working toward the M.S. degree in Fudan University, Shanghai, China.

TAO LIU was born in Sichuan, China, in 1992. He received the B.E. degree in information security from the University of Electronic Science and Technology of China, Chengdu, China, in 2014, and the master's degree from the University of Science and Technology of China (USTC). He is currently pursuing the Ph.D. degree in electronic information with Fudan University.

KAIPING YUAN received the Ph.D. degree from Fudan University, Shanghai, China, in 2019. He is currently a Young Associate Researcher with the Frontier Institute of Chip and System, Fudan University. He has been involved in the construction of new micro-nano smart gas sensors systems.

TIELIANG LV received the Ph.D. degree from the Institute of Microelectronics of Chinese Academy of Sciences, Beijing, China, in 2001. He is currently a Professor with the School of Microelectronics, Fudan University. He has been involved in the construction of instrumentation system with high reliability.